# Influence of Intrinsic Spin Ordering in $La_{0.6}Sr_{0.4}Co_{0.8}Fe_{0.2}O_{3-\delta}$ and $Ba_{0.6}Sr_{0.4}Co_{0.8}Fe_{0.2}O_{3-\delta}$ towards Electrocatalysis of Oxygen Redox Reaction in Solid Oxide Cell

Shoroshi Dey,[a,b#] Rajasekar Saravanan,[a#] Suprita Hati,[a] Soumyabrata Goswami,[c*] Athira Suresh,[d] Deepshikha Jaiswal-Nagar,[d] Moupiya Ghosh[e], Satadal Paul,[f] Abir Bhattacharya,[g] Madhumita Mukhopadhyay[h*] and Jayanta Mukhopadhyay[a, b*]

a. Energy Materials & Devices Division, CSIR-Central Glass and Ceramic Research Institute, Kolkata – 700032, India
b. Academy of Scientific and Innovative Research (AcSIR), Gaziabad-201002, India
c. Department of Chemistry, Amity Institute of Applied Sciences, Amity University, Kolkata-700135, India
d. School of Physics, Indian Institute of Science Education and Research Thiruvananthapuram, Kerala 695551
e. Department of Physics, Basic Science & Humanities, University of Engineering and Management, Newtown, Kolkata, West Bengal 700160, IndiaDepartment of Chemistry, Bangabasi Morning College, Kolkata, 700009, West Bengal, India
f. Department of Physics, The Bhawanipur Education Society College, University of Calcutta, 700020 Kolkata
g. School of Chemistry, University of St Andrews, St Andrews, Fife KY16 9ST, UK

[#] Share equal contribution as first author

* Correspondence to:

jmukhopadhyay75@gmail.com; jayanta_mu@cgcri.res.in (JM);
madhubanerji@gmail.com; mm613@st-andrews.ac.uk (MM) and
sgoswami423@gmail.com (SG)

## Supplementary document

### 1. Spin state equilibrium for $Co^{3+}$ ion

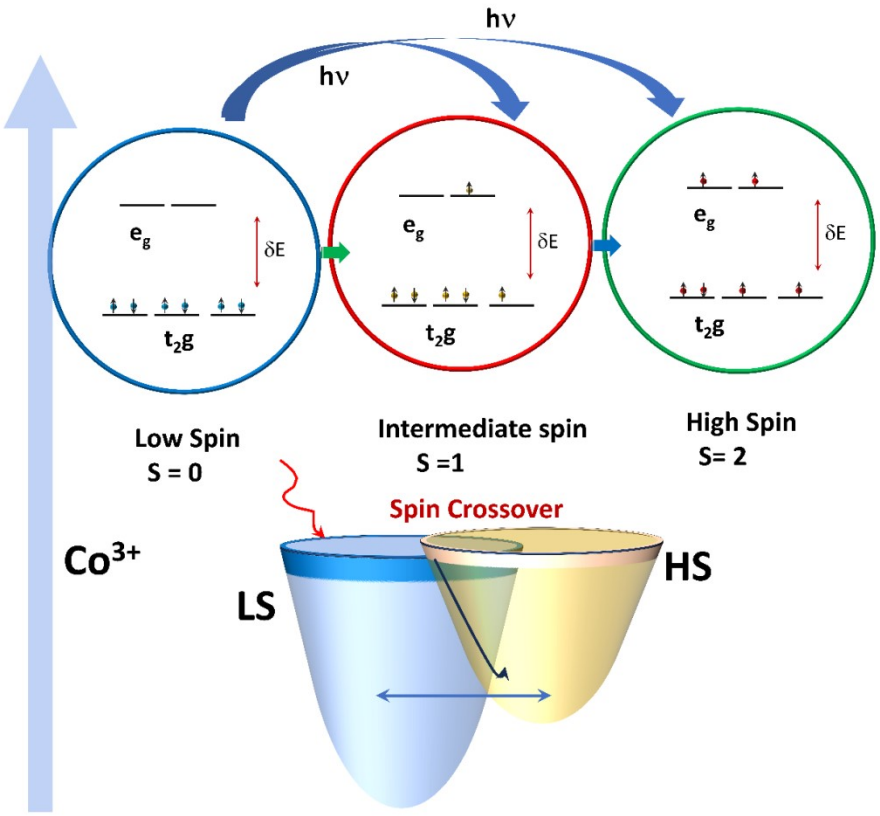


**Figure S1.** Schematic diagram for spin state equilibrium for $Co^{3+}$

Figure S1 shows the transition of lower to higher spin state exhibited by $Co^{3+}$ ion. The spin transitions of $Co^{3+}$ is facilitated by the interaction of lattice oxygen within the perovskite matrix (doped $SrCoO_3$). The thermal activation from initial spin state (S=0) to high spin induces magnetism within the system which shows significant super magnetism and magnetic ordering upon doping with $La^{3+}$, $Ba^{2+}$ at the A-site and $Fe^{3+}$ at the B-site. However, XPS confirms the formation of multiple oxidation states of the transition metal ions like $Co^{3+/4+}$, $Fe^{2+,/3+/4+}$ which participates during dissociation of fed oxygen (through air/oxygen) followed by diffusion and adsorption on the surface of electrocatalyst. These species promote the

surface exchange interaction for oxygen reduction and / oxygen evolution reaction during cell operation in either fuel cell or electrolyser cell mode. The primary aliovalency generation is noted in B-site elements as $BO_6$ octahedra is the active catalytic regime which is thermoenergetically influence by doping at A-site elements.

**2. Functionality of LSCF-6482 & BSCF-6482 using Partial Density of States**

The mechanistic influence of ligands viz. glycine, L-alanine and citric acid towards the functionalization of LSCF-6482 and BSCF-6482 is described in Figure S1. In the present context, an attempt is being pursued to correlate the functionality of LSCF-6482 and BSCF-6482 for application in SOFC and/or SOEC using density of states derived using theoretical quantum mechanics. The study involves the electronic structure determination of many body system using Gaussian 09 suite of quantum chemical program.

Figure S2 shows the density of states (DOS) plot as a function of spin state for LSCF-6482 and BSCF-6482. This study has been initiated through geometry optimization of both the pristine and doped perovskites followed by quantum mechanical calculations. Owing to significant semiconducting regions, both conduction and valence band regime coexists in all DOS plot. The majority of spin channel contains a flat region of spin states in the middle energy range thereby spanning the energy states. These states are possibly hybrid TM3d (TM: transition metal) and O2p states. The reported sample reveals three specific binding energy regimes for distribution of electron density [bonded regime (-19 to -16 eV), valence regime (-8 to 0 eV) and conduction band (0- 50 eV)] separated by a nodal zone ($\Psi^2$ {electron density} = 0). The primary driving force for difference in functionality in LSCF and BSCF is based on charge compensation and hole creation due to aliovalent and isovalent substitutions. Aliovalent doping of $La^{3+}$ within $Sr^{2+}$ generates unit negative charge owing to which holes are created upon neutralizing the formed negative charge (Eq. 1). The produced holes tend to

delocalize partially to oxygen sublattice to form the oxygen vacancies ($V_o^{\circ\circ}$) wherein two substitutions (equivalent to two negative charge) account for the generation of single oxygen vacancy ($V_o^{\circ\circ}$).

$$Aliovalent\ doping \overset{2Sr^{2+}\ in\ A\ site}{\rightarrow} 2LaCoO_3 \Rightarrow 2Sr_{La}^{'} + V_o^{\circ\circ} \quad (1)$$

Relevant positions in Oxygen (2p) with respect to Co (3d) / Fe (3d) states becomes the governing factor for positioning the generation of Oxygen vacancy [Co-$V_o^{\circ\circ}$-Co] or [Fe-$V_o^{\circ\circ}$-Fe]. $V_o^{\circ\circ}$ sites preferably occupy oxygen sites present in between Co-O-Co in comparison to Fe-O-Fe whose oxygen vacancy formation energy ($\Delta E_{fvac}$) is more compared to the latter. This signifies that in LSCF and BSCF, formation of oxygen vacancy is more prone in $CoO_6$ octahedra compared to $FeO_6$. In order to promote the catalyst activity for OER/ORR, charge compensation using ion pairs and oxygen vacancy should maintain a non-steady state equilibrium. Therefore, in addition to either iso or aliovalent substitution at '*A*' site, $Fe^{3+}$ is substituted in 20 % proportion at the B-site. The ionic equilibrium (Eq. 1) also promotes disproportionation reaction at Co-site (Eq. 2) which is governed by the type of iso/aliovalent substitution. $Doped\ Perovskite\ (LaCoO_3) \overset{2Sr^{2+}\ in\ A\ site}{\rightarrow} \overset{2\ Fe^{3+}\ in\ B\ site}{\rightarrow} 2Sr_xLa_{1-x}O_3$

$$\Rightarrow 2Sr_{La}^{'} + V_o^{\circ\circ} + 2Co_{Co}^{'}\ \ i.e\ Co_{Co}^{'} \Longrightarrow Co^{3+} \leftrightharpoons Co^{2+} + Co^{4+} \quad (2)$$

Using **Eq. 2**, two simultaneous reactions can be highlighted as:

$$Fe_{Fe}^{\circ}\ or\ Co_{Co}^{'} \overset{(route\ 2)\ B\ site}{\leftarrow} 2Sr_xLa_{1-x}O_3 \overset{A\ site\ (route\ 1)}{\rightarrow} 2Sr_{La}^{'}$$

$$2Sr_xLa_{1-x}O_3 \overset{route\ 3}{\rightarrow} V_o^{\circ\circ} \Rightarrow Co - V_o^{\circ\circ} - Co\ (Minor\ fraction) + Fe - V_o^{\circ\circ} - Co\ (Major\ fraction) \quad \textbf{(3)}$$

Reaction mechanism involve simultaneous route 1, 2 and 3 wherein charge compensation proceeds through a charge transfer and/or oxygen vacancy mode. The controlling parameter is mainly reported as the substitution at the A site which form the network builder. It has been reported that, primary charge carriers are the aliovalent states prevalent at all A and B sites

elements. Furthermore, aliovalent substitution at A site ($Sr^{2+}$) promotes the formation of Co-$V_o^{\circ\circ}$-Fe which act as vacancy trap (Eq. 5, LHS driven reaction) compared to Co- $V_o^{\circ\circ}$-Co (promotes oxygen vacancy generation and propagation).

$$2Co_{Co}^{x} + O_O^x \rightleftharpoons 2Co_{Co}^{'} + V_o^{\circ\circ} + {}^1/_2\ O_2 \quad (4)$$

$$2Fe_{Fe}^{x} + O_O^x \rightleftharpoons 2Fe_{Fe}^{'} + V_o^{\circ\circ} + {}^1/_2\ O_{2\,(g)} \quad (5)$$

It can be stated from Figure S2a, that the principal quantized energy distribution as a function of either α/β spin state for $ABO_3$ system is independent of B-site element whereas, significantly varied DOS plots are observed by variation of 'A' site (La, Sr and Ba) with a constant B-site either Co and/Fe in Figure S2).

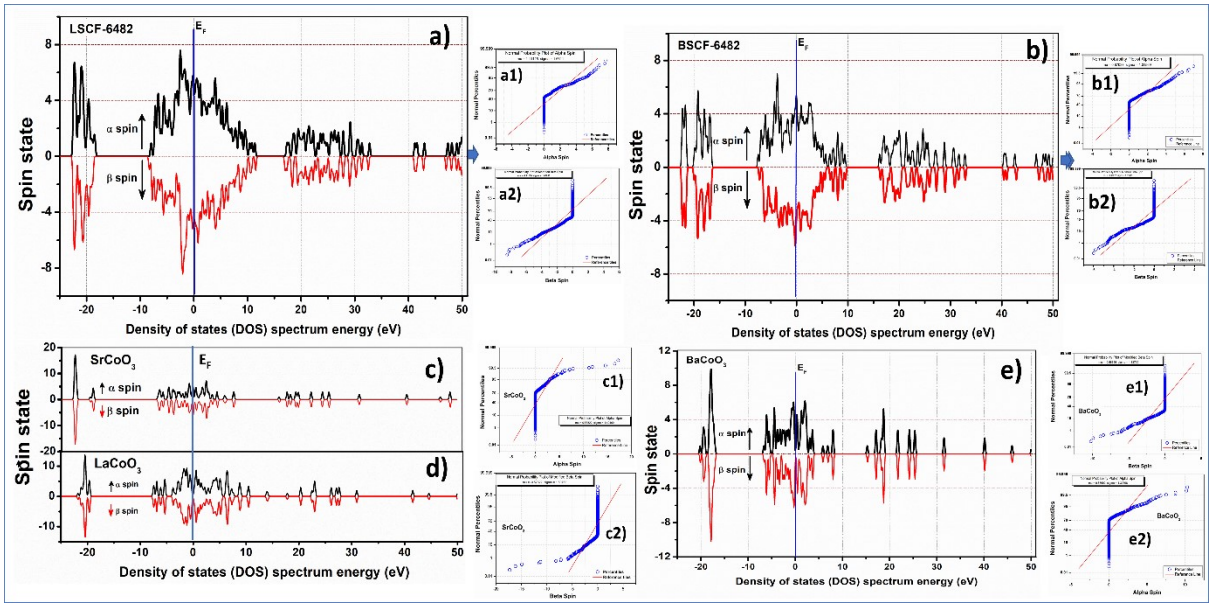


**Figure S2.** PDOS plots as a function of spin states for: a) LSCF-6482, b) BSCF-6482, c) $SrCoO_3$, d) $LaCoO_3$ and e) $BaCoO_3$. The respective normal probability plot for spin states of the PDOS are shown in (a1, a2); (b1, b2); (c1, c2); (d1, d2); (e1, e2).

The distribution of electron density within a fixed binding energy zone is found to get modulated by: a) B-site elements and b) % doping and nature of element doped in B-site. It can be noted from comparative DOS plots of pristine and doped compositions, that the degree

of delocalization (represented generally by $\lambda_{deloc}$) of electronic charge accelerates in a doped sample as shown in the normal probability plots in Figure S2 (a1, a2); (b1, b2). This is indicated by much reduced nodal regimes ($\Psi^2 \neq 0$) within the Zone 2 (binding energy regime of -7 to 0 eV) which are primarily dictated by O2p orbitals and also within the conduction band (Zone 3). The extent of charge delocalization is observed to be maximum within -10 to 10 eV within the merged zone of 2 and 3 (separated by Fermi energy $E_F$) and 15 to 30 eV within the conduction zone. The direct correlation of such charge delocalization is also manifested in much negative single point energy for doped LSCF-6482 and BSCF-6482 as determined through quantum calculations and reported in Table S1.

Table S1. Single point energy of pristine and doped perovskite system computed from DFT

| **System** | **Single point energy (AU)** *1 Hartree = 27.211 eV* |
|---|---|
| $SrFeO_3$ | -818.18282902 AU = -22263.573 eV |
| $SrCoO_3$ | -839.81654101 AU = -22852.2479 eV |
| $LaFeO_3$ | -824.70873843 AU = -22441.1495 eV |
| $LaCoO_3$ | -846.36701558 AU = -23030.4928 eV |
| $BaFeO_3$ | -776.56796497 AU = -21131.1909 eV |
| $BaCoO_3$ | -798.20477260 AU = -21719.9501 eV |
| LSCF-6482 | -1405.13152746 AU = -38235.0338 eV |
| BSCF-6482 | -1368.83816483 AU = -37247.4552 eV |

The probability of zonal compensation of charge through ion pair formation is limited in BSCF-6482 which is indicated by limited nodal or node like area where $\Psi^2$ is close to zero. The two regimes (bonded and valence) within the BSCF system are widely spread (shown by max $\Psi^2$ magnitude). This signifies better charge compensation by oxygen ion vacancy that requires more nodal free zone (s). On the contrary, LSCF system allows ion pair formation and does not prefer to accelerate oxygen ion vacancy as indicated by more negative energy

(initiated from -8.5 eV compared to – 7 eV for LSCF) in the valence band. This allows better electronic conduction in LSCF as an air electrode functionality in SOFC, whereas BSCF activates its function through oxygen vacancy. In contrast to LSCF, isovalent ion substitution in BSCF bear less probability of ion compensation through aliovalency within A and/or B site elements owing to which ion pair formation gets restricted and the disproportionation reaction (Eq. 2) is less probable which favour the concentration density of Co- $V_o^{\circ\circ}$-Co. The generation of oxygen vacancy, sustenance and propagation is higher in BSCF-6482 with comparatively lesser extent of charge compensation by oxidation state aliovalency. In BSCF, generation of Co-$V_o^{\circ\circ}$-Co leads to charge redistribution around the vacant sites. Energetically, at higher oxygen vacancies total vacancy formation energy tends to linearly accelerate which results in structural / lattice expansion from cubic system.

The study on density of states as a function of electronic spin is derived out of orbital splitting as shown in some representative Figure S3. The respective DOS pristine system (Figure S3c-d) has been initially studied and reported by Dey et al.[1] It is to be mentioned that, in case of pristine system, irrespective of B-site element, incorporation of La and Sr tend to have more attractive/ stable HOMO which results in much higher single point interactive energy of -23 x$10^3$ eV compared to Ba based oxides (-21 x$10^3$ eV). Incorporation of less penetrating *f* orbital in LUMO is more prevalent with La family after spitting degeneracy owing to which accelerated electronic conduction/MIEC behaviour through ion pair is more pronounced upon doping La in LSCF-6482. The single point optimized energy for doped system is still higher compared to the pristine compositions which support further stability of the systems though loss in orbital degeneracy. However, during the computation of DOS, the doped systems are iterated and found to be devoid of any symmetry operation owing to which the splitted orbital degeneracy are all denoted to be of even singular symmetry (denoted by ***A***). The lesser stabilization of BSCF system (low single point energy compared to LSCF) and

presence to more screened orbitals at the LUMO level restricts the charge migration through aliovalency. However, as seen from the orbital plot of pristine $BaBO_3$ and $SrBO_3$ [B refers to either Co/Fe], the high energy LUMO is composed of single (odd or even symmetry), double and triple (A, B, C and T) symmetry orbitals which are reported to be more compatible to be hybrid orbital thereby allowing relaxation of quantum selection rules. Owing to such fact, generation of oxygen vacancy and charge compensation is more probable. This allows BSCF-6482 to be more effective in SOEC as also depicted in the impedance and performance evaluation of single cell.

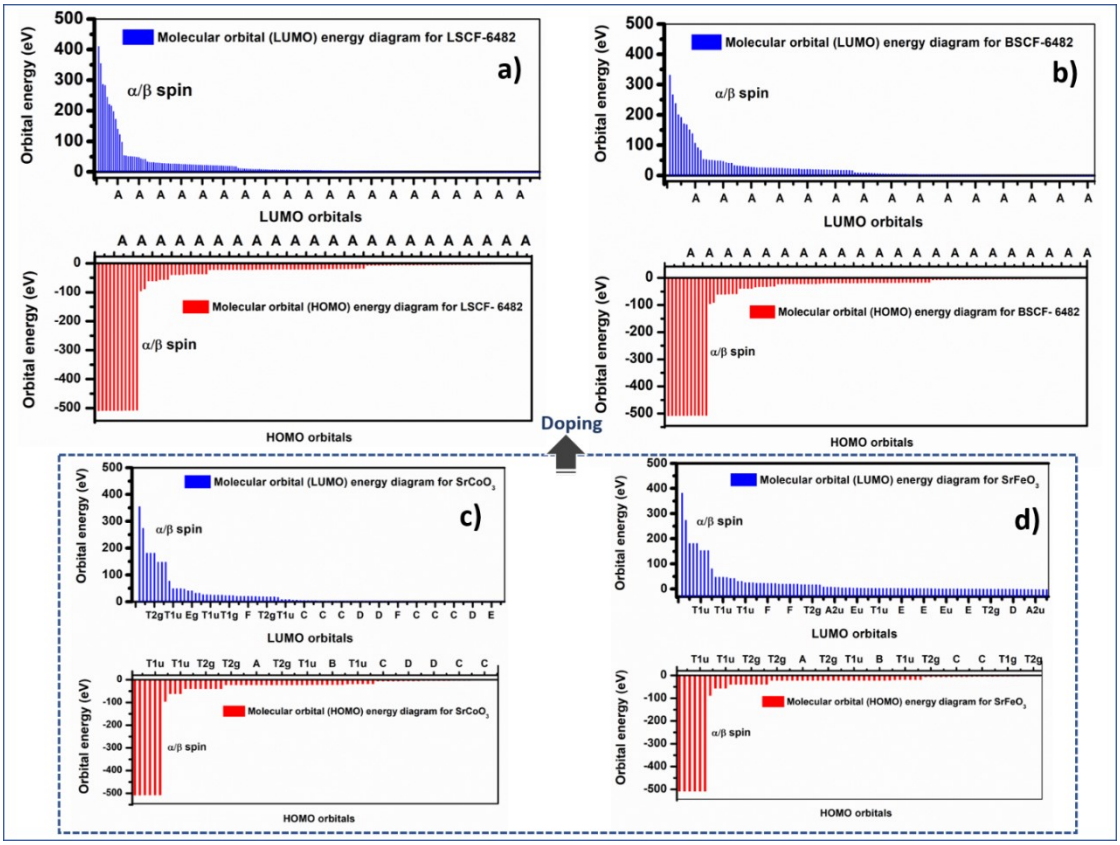


**Figure S3** Computed orbital energy as a function of associated HOMO & LUMO orbitals for: a) LSCF-6482, b) BSCF-6482, c) $SrCoO_3$ and d) $SrFeO_3$

## 2. Electrochemical impedance spectroscopy (EIS) for single cells fabricated with BSCF6482/LSCF6482

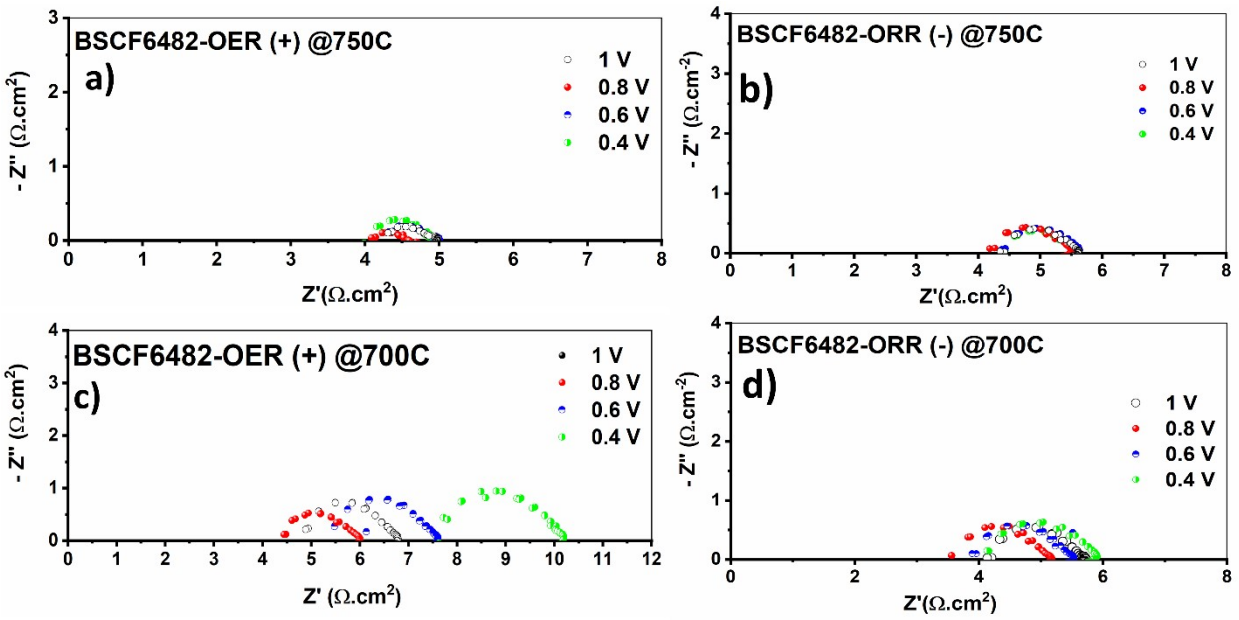


**Figure S4.** Nyquist plots for the single cells with BSCF6482 as the active electrocatalyst at an operating temperature of 750°C (a, b) and 700°C (c, d) as a function of applied potentials (0.4V-1.0V) for a), c) anodic (OER) and b), d) cathodic (ORR) bias.

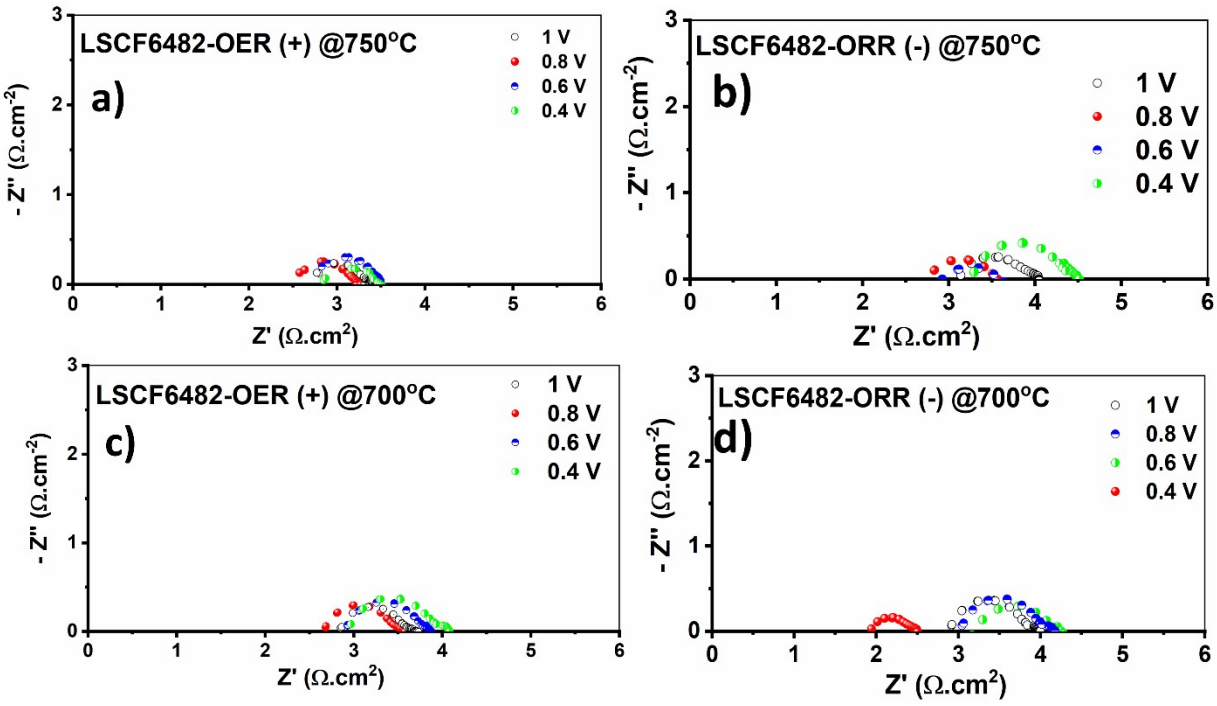


**Figure S5.** Nyquist plots for the single cells with LSCF6482 as the active electrocatalyst at an operating temperature of 750°C (a, b) and 700°C (c, d) as a function of applied potentials (0.4V-1.0V) for a), c) anodic (OER) and b), d) cathodic (ORR) bias.

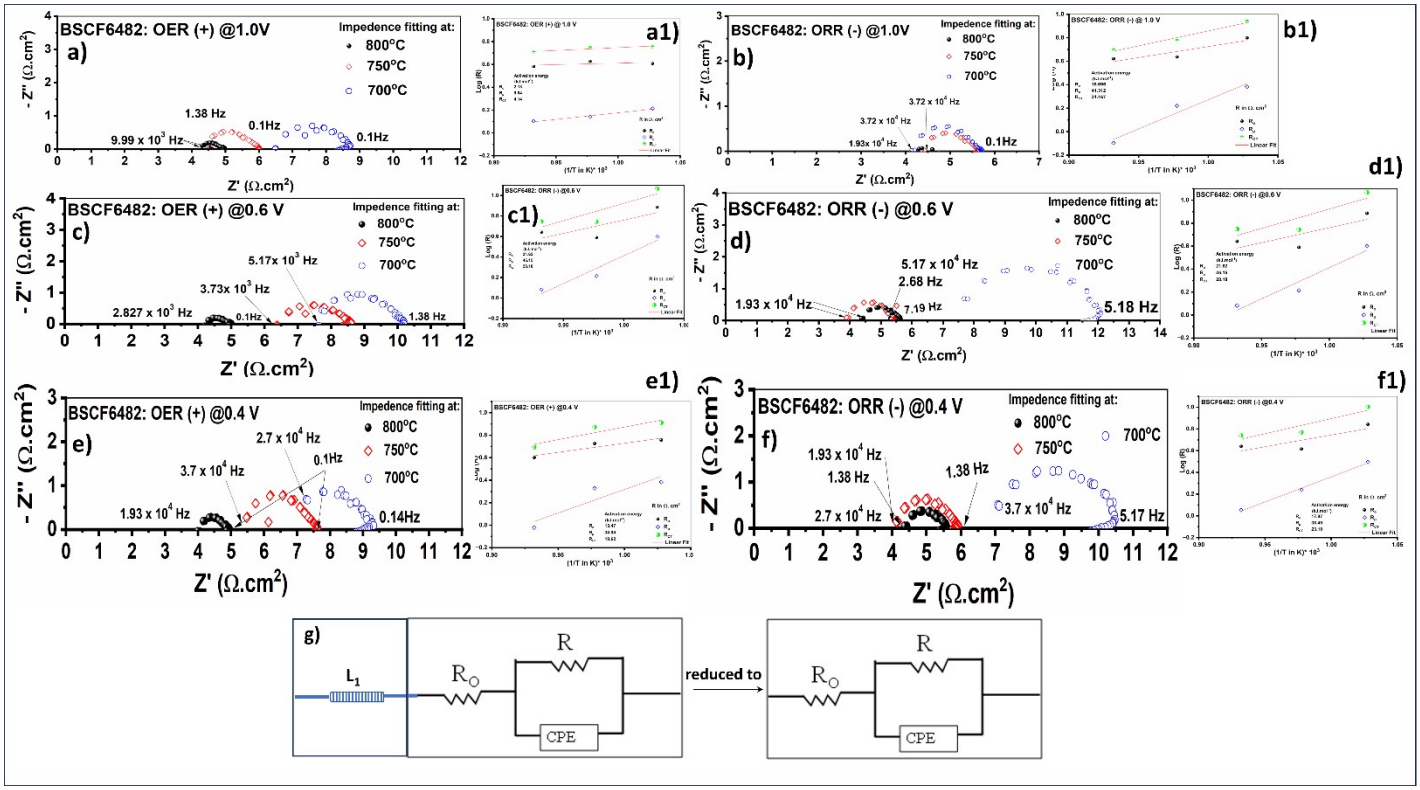


**Figure S6.** Impedance response of single cells fabricated using BSCF6482 in the temperature range of 700-800°C under anodic potential (+) of 1.0 V (a), 0.6 V(c) and 0.4 V (e) and cathodic potential (-) of 1.0 V (b), 0.6 V (d) and 0.4 V(f).

The activation energy plot for associated polarizations ($R_o$, $R_p$ and $R_{CT}$) for anodic potential (+) of 1.0 V (a1), 0.6 V(c1) and 0.4 V (e1) and cathodic potential (-) of 1.0 V (b1), 0.6 V (d1) and 0.4 V(f1). The corresponding equivalent circuit is shown in g).

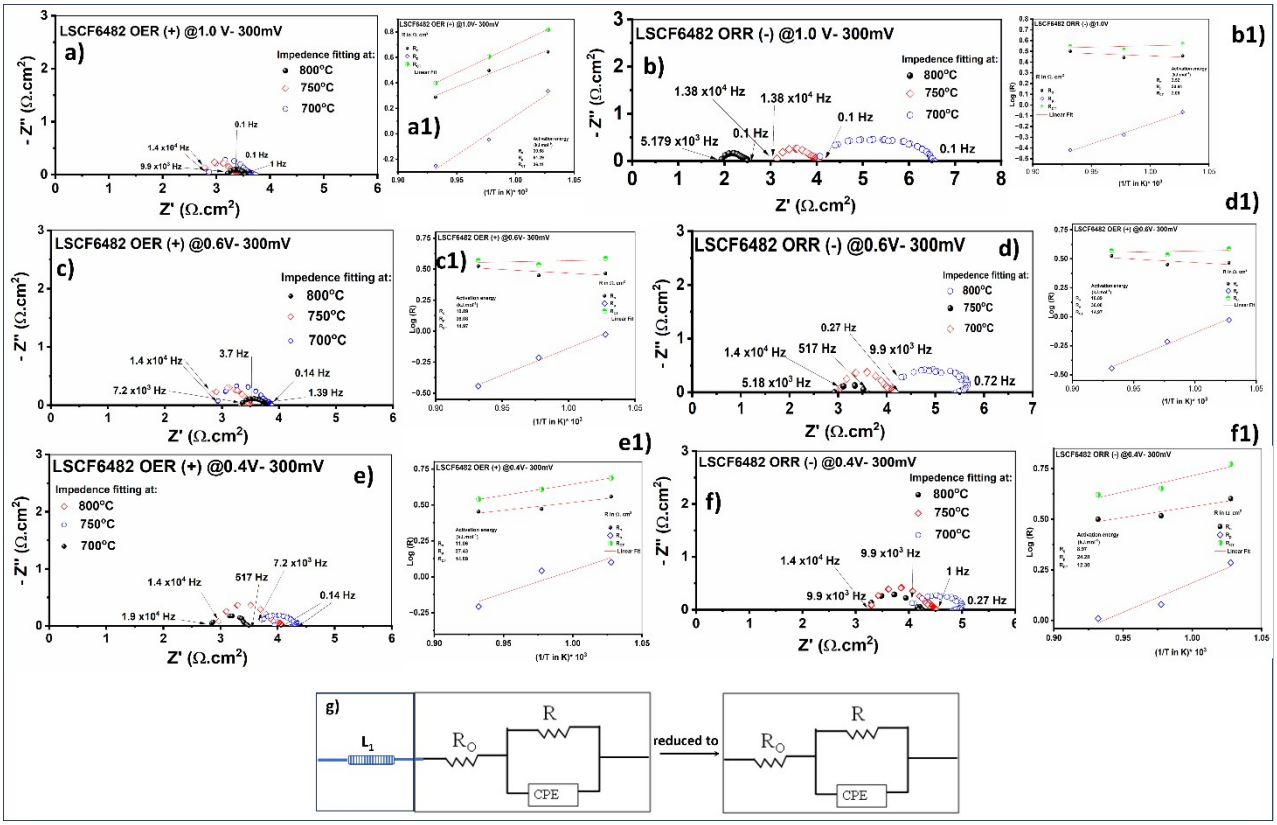


**Figure S7.** Impedance response of single cells fabricated using LSCF6482 in the temperature range of 700-800°C under anodic potential (+) of 1.0 V (a), 0.6 V(c) and 0.4 V (e) and cathodic potential (-) of 1.0 V (b), 0.6 V (d) and 0.4 V(f).

The activation energy plot for associated polarizations ($R_o$, $R_p$ and $R_{CT}$) for anodic potential (+) of 1.0 V (a1), 0.6 V(c1) and 0.4 V (e1) and cathodic potential (-) of 1.0 V (b1), 0.6 V (d1) and 0.4 V(f1). The corresponding equivalent circuit is shown in g).

The equivalent circuit fitted composed of an inductor couple with resistors (ohmic contribution and polarization resistance) connected in parallel to the capacitive part of the circuit viz CPE. Since, the inductor part is very small, the circuit is simplified with removal of the inductor component as shown in Figure S6g and S7g.

4. **Kinetic and Mechanistic Analyses on the influence of A-site doping of $SrFeO_3$**

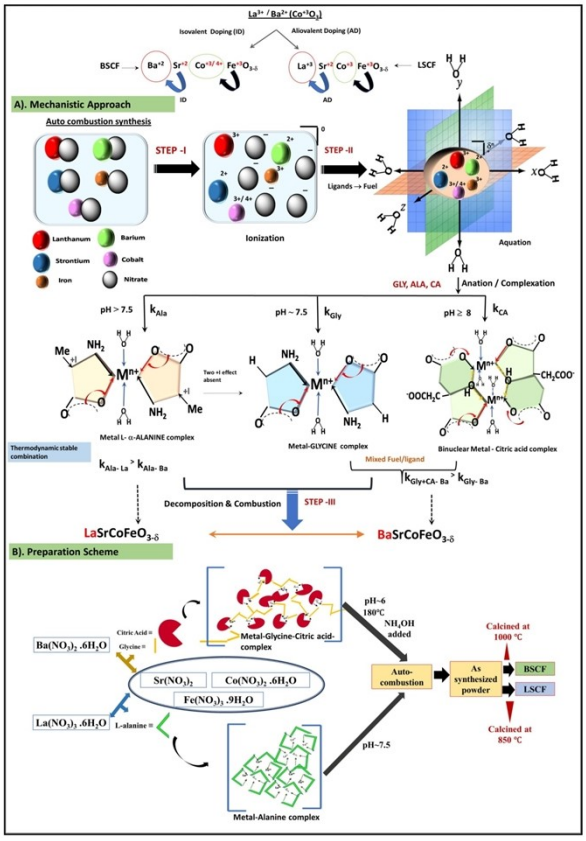


**Fig. S8.** a) Schematic for mechanistic approach (including thermodynamic and kinetic factors) for auto combustion synthesis and b) preparation steps for solution combustion synthesis of doped $SrFeO_3$ system.

References


1. Shoroshi Dey, Debosreeta Bose, Yuksel Akinay, Madhumita Mukhopadhyay, Abhijit Das Sharma, Jayanta Mukhopadhyay, Elsevier Series in Advanced Ceramic Materials, Surface Modification and Functionalization of Ceramic Composites, 2023, 255-288, ISBN 9780323858830, https://doi.org/10.1016/B978-0-323-85883-0.00021-1.